Surface and porosity of nanocrystalline boehmite xerogels

Pierre Alphonse [a] and Matthieu Courty [a]

[a] CIRIMAT, UMR-CNRS 5085, Université Paul Sabatier, 118 route de Narbonne, 31062 Toulouse Cedex 04, France

Abstract

Boehmite xerogels are prepared by hydrolysis of $Al(OC_4H_9)_3$ followed by peptization with HNO_3 ($H^+/Al = 0$, 0.07, 0.2). XRD and TEM show that these gels are made of nanosized crystals (5–9 nm in width and 3 nm thick). According to the amount of acid, no significant differences are found in size and shape, but only in the spatial arrangement of the crystallites. Nitrogen adsorption–desorption isotherms of nonpeptized gels are of type IV, whereas isotherms of peptized gels are of type I. These isotherms are analyzed by the *t*-plot method. The majority of pore volume results from intercrystalline mesopores, but the peptized gels also contain intercrystalline micropores. The particle packing is very dense for the gel peptized with $H^+/Al = 0.2$ (porosity = 0.26), but it is less dense in non-peptized gel (porosity = 0.44). Heating these gels under vacuum creates, from 250 °C onwards, an intracrystalline microporosity resulting from the conversion of boehmite into transition alumina. But heating also causes intercrystalline micropores collapsing. The specific surface area increases up to a limit temperature (300 °C for nonpeptized gels and 400 °C for peptized) beyond which sintering of the particles begins and the surface decreases. The PSD are calculated assuming a cylindrical pore geometry and using the corrected Kelvin equation proposed by Kruk et al. Peptized xerogels give a monomodal distribution with a maximum near 2 nm and no pores are larger than 6 nm. Nonpeptized gels have a bimodal distribution with a narrow peak near to 2 nm and a broad unsymmetrical peak with a maximum at 4 nm. Heating in air above 400 °C has a strong effect on the porosity. As the temperature increases, there is a broadening of the distribution and a marked decrease of small pores (below 3 nm). However, even after treatment at 800 °C, micropores are still present.

Keywords: Boehmite; Specific surface area; Porosity; PSD; Comparative plot

1. Introduction
2. Experimental
2.1. Synthesis
2.2. Characterization
3. Results and discussion
3.1. Loss on ignition
3.2. XRD of boehmite xerogels
3.3. TEM observation on boehmite xerogels
3.4. Density of boehmite xerogels
3.5. Pore size analysis of boehmite xerogels
3.6. Effect of dehydration on the porosity of boehmite xerogels

4. Summary
Acknowledgements
References

1. Introduction

Boehmite, aluminum oxyhydroxide (AlOOH), is a versatile material employed in domains such as sol–gel ceramics, surface coatings, rheology control, and pharmaceuticals. But it is also widely used as a precursor of alumina, which widens its application field to refractories, abrasives, cements, catalysts, adsorbents, membranes, etc. In most of these applications control of the specific surface area and the porosity is essential.

According to its crystal size, boehmite has very different morphologies, porosities, and surface areas so that nanocrystalline boehmite was thought to be a distinct form, called pseudoboehmite (or gelatinous boehmite) [1] and [2]. However, recent crystallographic studies [3], [4], [5], [6] and [7] have clearly demonstrated that pseudoboehmite is simply nanocrystallized boehmite. It has been shown by Lippens [8] that the internal surface area formed by dehydration on heating strongly depends on the particle size of boehmite: the smaller the crystals, the smaller the increase of the surface area. This is because the dehydration is pseudomorphic. If crystallite size is large (small specific surface area), when water is expelled, space will be created in the particle, which thus becomes microporous because the external volume of particles does not change very much [9], [10] and [11]. Conversely, in the case of nanocrystalline boehmite, the crystallites are so small that the collapse of the structure during the expulsion of the water leads to particle shrinkage and does not create significant internal porosity.

Nanosized boehmite can be prepared by solution chemistry processes such as neutralization of aluminum salts or alkoxide hydrolysis [1]. The latter method leads to a very pure hydroxide and it is often used in the sol–gel synthesis of alumina. In the well-known method of Yoldas [12], [13], [14] and [15], the hydroxide is peptized into a colloidal solution (sol) by the addition of acid. Yoldas has shown that the volume of the gel at the gelling point goes through a minimum for a given acid amount. It is for this minimum that the resulting xerogel has optimal properties (porosity, mechanical strength), because less shrinkage occurs during drying.

The main goal of this study was to work out, mainly from a detailed analysis of the nitrogen adsorption–desorption isotherms, the effect of the peptization, the water content, and the transformation in transition alumina on the texture of boehmite xerogels synthesized by the Yoldas process.

2. Experimental

2.1. Synthesis

Three kinds of boehmite xerogels were synthesized according to the process originally reported by Yoldas [12], [13], [14] and [15]. A large excess ($H_2O/Al \approx 100$) of hot (85 °C) distilled water was quickly poured into aluminum tri-*sec*-butoxide, $Al(OC_4H_9)_3$, under vigorous stirring, which was maintained for 15 min. The samples of the first type (S1) were not peptized. For the second type (S2), the hydroxide precipitate was peptized by adding 0.07 mole of nitric acid (aqueous solution of 7% by weight HNO_3) per mole of alkoxide and stirring at 85 °C until a clear sol was obtained (~24 h). For the third type (S3), peptization was done with 0.20 mole of nitric acid per mole of alkoxide. After peptization, the sols were concentrated by heating at 85 °C until 2/3 of the solvent had evaporated. Finally, xerogels were prepared by drying concentrated sols (or hydroxide precipitates) in air at various temperatures from 20 to 150 °C.

2.2. Characterization

The crystal structure was investigated by powder X-ray diffraction (PXRD). Data were collected on a Seifert 3003TT θ–θ diffractometer in Bragg–Brentano geometry, using filtered CuK* radiation and a graphite secondary-beam monochromator. Diffraction intensities were measured by scanning from 5 to 90° (2θ) with a step size of 0.02° (2θ). For pattern decomposition the reflection profiles were modeled by pseudo-Voigt functions. The peak positions were constrained by lattice parameters. A separate set of parameters—peak intensity, full width at half maximum (FWHM), Lorentzian fraction of pseudo-Voigt function—was used to model each diffraction profile.

Transmission electron microscopy (TEM) analyses were done on a JEOL 2010. A small amount of sample powder was dispersed in ethanol using an ultrasound bath. Then the carbon-coated grid was dipped into the suspension and allowed to dry at room temperature.

The nitrogen adsorption–desorption isotherms were determined at 77 K, by a volumetric method with a Micromeritics ASAP 2010M. This system has 1000-, 10-, and 1-Torr pressure gauges and a turbomolecular pump. The isotherms were recorded in a wide range of relative pressures (10^{-5} to 0.995). Nitrogen of high purity (99.999%) was used. Sample tubes were equipped with a seal frit with built-in check valve. Thus the gels can be weighed after outgassing without any contamination by atmospheric air.

Skeletal densities of powder were measured using a gas pycnometer (Micromeritics AccuPyc 1330) and working with helium. Each experimental value results from the average of 10 successive measurements on the same sample.

3. Results and discussion

3.1. Loss on ignition

The loss on ignition (LOI), which corresponds to the percentage of water, was calculated from the mass loss measured after calcination of the xerogels at 1200 °C for 2 h. This treatment converts boehmite into *-alumina, Al_2O_3, according to the reaction

(1)
$2AlOOH \rightarrow H_2O + Al_2O_3$.

The expected mass loss for anhydrous boehmite AlOOH is 15%. But our xerogels contained much more (Table 1), especially those dried near room temperature. It is now admitted that the excess of water in boehmite is adsorbed on the crystallite surface, mainly because the quantity of water decreases when the crystallite size increases, becoming close to zero for large crystals [16], [17], [18] and [19]. For water proportions exceeding 25% multilayer adsorption should be considered.

Table 1.

Characteristics of boehmite xerogels

	S1-a	S1-b	S2-a	S2-b	S2-c	S3-a
T_{drying} (°C)	50	20	150	30	20	50
LOI = wt% H_2O	30.5	39.0	28.5	42.0	49.0	32.0
Al_2O_3 (wt%)	69.5	61.0	71.5	58.0	51.0	68.0
AlOOH (wt%)	81.8	71.8	84.1	68.2	60.0	80.0

	S1-a	S1-b	S2-a	S2-b	S2-c	S3-a
a (nm)	0.287	0.287	0.287	0.286	0.287	0.287
b (nm)	1.224	1.222	1.228	1.227	1.223	1.226
c (nm)	0.371	0.371	0.371	0.372	0.371	0.372
Crystal density (g cm^{-3})	3.06	3.07	3.04	3.05	3.06	3.04
2θ shift (°)	1.03	0.95	0.63	0.83	0.82	0.81
D(200) (nm)	5.6	5.8	7.1	4.8	6.2	6.9
D(020) (nm)	3.0	2.6	3.0	2.4	2.5	2.7
D(002) (nm)	7.1	7.5	6.1	9.2	5.8	6.1
Experimental density (g cm^{-3})	2.36	2.10	2.48	2.03	1.81	2.38

3.2. XRD of boehmite xerogels

The X-ray diffraction patterns of typical samples are reported in Fig. 1. Except for the first reflection, they appear to be very similar. The broad diffraction lines reveal that the crystallites are very small. The boehmite structure corresponds to an orthorhombic unit cell. The diffraction peaks have been indexed using the space group Cmcm. Pattern decomposition of the experimental diagrams gives good agreement with the boehmite structure provided that the first line (020) is excluded, because it presents too large a shift toward small angles from its calculated position (see Table 1). This shift of the (020) line, observed for microcrystalline boehmite, can be explained essentially by a particle-size effect [3], [4] and [19]. The values of the cell parameters corresponding to the best fit are very similar for the three kinds of xerogels and the various amounts of water (Table 1). Moreover they are close to the parameters reported in the literature (*a*=0.2868 nm; *b*=1.2214 nm; *c*=0.3694 nm) for well-crystallized boehmite [20], which demonstrates that water excess has little effect on the crystal structure.

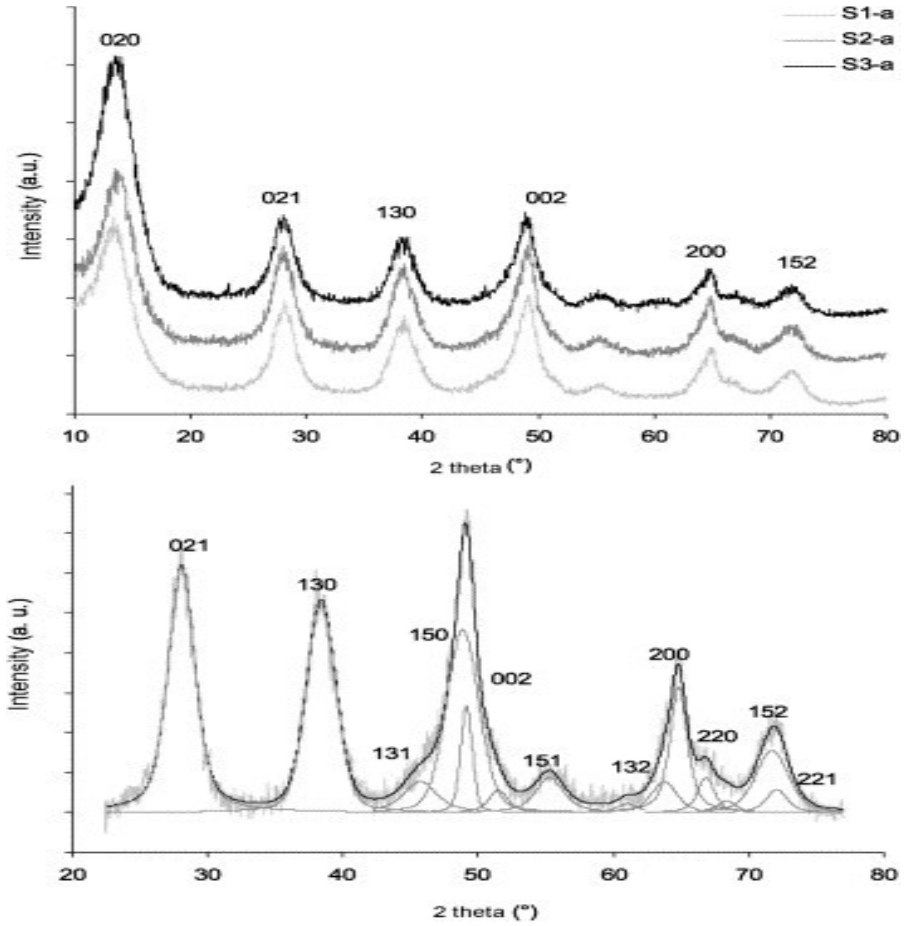

Fig. 1. X-ray diffraction patterns of boehmite samples (Cu*K** radiation) with an example of a pattern decomposition (orthorhombic unit cell, space group No. 63, Cmcm).

The widths of the 002 and 200 reflections are smaller than the others because the crystallite dimensions along the *a* and *c* axes are larger than that along the *b* axis, which means that the crystallites are in the shape of platelets or disks. Such a shape has often been reported for microcrystalline boehmite. The refined FWHM of the 200, 020, and 002 lines can be used to estimate, by Scherrer's equation, the average crystallite size along the *a*, *b*, and *c* axes. The instrumental broadening contribution was evaluated by using *-alumina (S2 calcinated at 1400 °C for 2 h) as standard. The results, reported in Table 1, show that the thickness is in the range 2.5 to 3 nm. The length (along the *c* axis) is in the range 6 to 9 nm and the width is in the range 5 to 7 nm.

The marked enhancement in intensity of the 020 diffraction line indicates that a large proportion of the crystallites have their *b* axes oriented in a direction close to the normal to the sample holder plane. This texture is due to the plate shape of the crystallites and has already been reported [21], [22] and [23] for microcrystalline boehmite.

3.3. TEM observation on boehmite xerogels

TEM micrography (Fig. 2a) of a S3 sol at low concentration gives further evidence of the very small size of the crystallites. Nanocrystals of 3–4 nm can be seen, but they stick together to build polycrystalline objects, mainly fibers. It can be noted that the fibers themselves do not stick; a space

of about 1 nm is maintained, which creates a microporous network (Fig. 2b). In S1 gels the elementary nanocrystals give, in addition, bidimensional objects (sheets), often folded (Fig. 2c). S2 presents behavior intermediate between S1 and S3. The size of the elementary nanocrystals is in acceptable agreement with the size of the coherent diffraction domains observed by XRD.

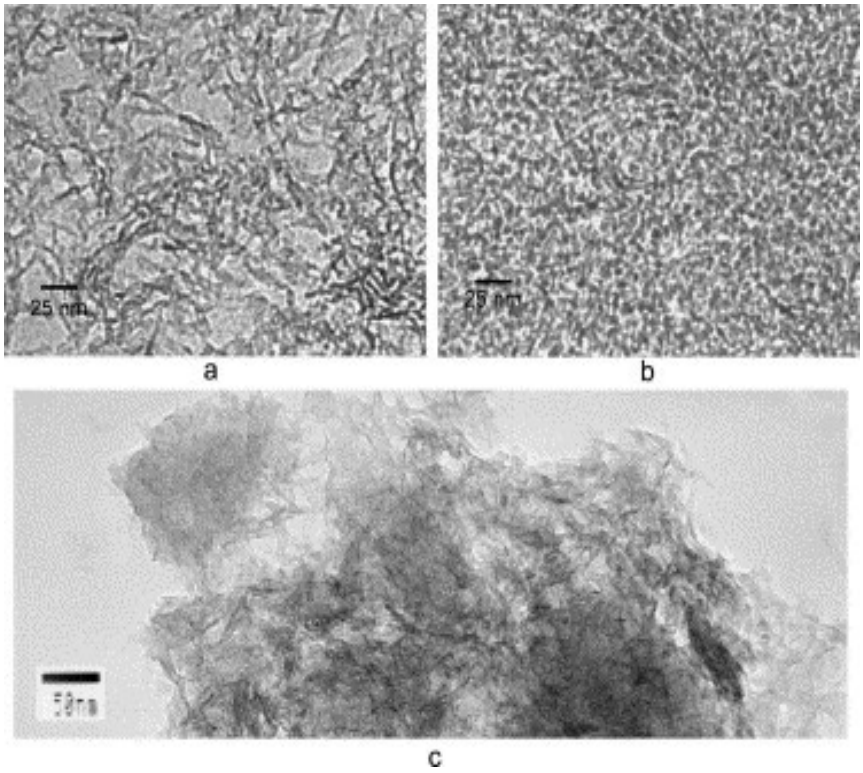

Fig. 2. TEM micrographs of boehmite xerogels. (a) sol S3-a at low concentration; (b) sol S3-a at higher concentration; (c) sol S1-b.

The differences inhe microstructure of the gel, according to the amount of acid added after hydrolysis, can be explained by the electrostatic repulsion between the boehmite particles. The surface of boehmite synthesized in water is fully covered by hydroxyl groups. These surface hydroxyl groups have an amphoteric character; thus the surface may become positively or negatively charged depending on the pH,

$$\equiv Al\_OH + H^+ \leftrightarrow \equiv Al\_OH^+_2,$$

$$\equiv Al\_OH + OH^- \leftrightarrow \equiv Al\_O^- + H_2O,$$

where $\equiv$Al_OH represents a surface hydroxyl group. The pH at which the overall charge of the water–oxide interface is close to zero is known as the point of zero charge (PZC). For boehmite powder, the PZC reported in the literature is close to 9 [24] and [25]. In nonpeptized gels (S1) the pH is close to 8, which is near to the PZC, and the surface charge is low. The particles will stick together to build bidimensional objects (sheets). When acid is added the surface charge will increase, leading to increased electrostatic repulsion between the particles. They will now organize in monodimensional objects (fibers) and if the amount of acid is enough even elementary particles will be separated. When boehmite particles become smaller than the visible light wavelength the sol appears transparent. Yoldas [14] has shown that at least 0.03 M of acid per mole of alkoxide must be added to obtain a clear sol. The surface charges prevent the collapse of the structure during the sol–gel transition and the further drying into a xerogel. So the space observed between the particles in the micrography is probably due to electrostatic repulsion.

3.4. Density of boehmite xerogels

The skeletal densities of boehmite xerogel powders have been determined using a gas pycnometer and working with helium. From the cell parameters we have calculated the cell volume and then the crystal density. There is a strong discrepancy between experimental densities and the densities calculated from the lattice parameters (Table 1). This difference can be related to the amount of water contained in the xerogels, as shown in Fig. 3, where the experimental densities have been plotted against $\%H_2O$. Clearly there is a relationship between density and water excess. Density is the ratio of the mass to the volume; thus the crystal density, calculated from the lattice parameters, is

(4)

$$\rho_{crystal} = \frac{m_{crystal}}{V_{crystal}}.$$

Similarly an estimated density, taking into account the volume occupied by the water excess, can be calculated:

(5)

$$\rho_{est} = \frac{m_{H_2O} + m_{crystal}}{V_{H_2O} + V_{crystal}}.$$

For a sample mass of 1 g, $m_{H2O}+m_{crystal}=1$, which gives

(6)

$$\rho_{est} = \left(V_{H_2O} + \frac{1 - m_{H_2O}}{\rho_{crystal}} \right)^{-1}$$

with $m_{H2O}=1-\%AlOOH/100$. If we assume that the volume taken by 1 g of water is equal to 1 cm^3 then $V_{H2O}=m_{H2O}$. The results are reported in Table 1. The estimated densities are lower than the experimental values but the agreement can be improved if we assume that the volume taken by 1 g of water is less than 1 cm^3. For example, the plot for a specific volume of 0.9 cm^3/g has been reported in Fig. 3. Actually the volume leading to a good agreement decreases together with the water content. As the heat of water adsorption on alumina decreases with the surface coverage [26], this reduction of the volume could be related to an increase of the interaction between water and the boehmite surface.

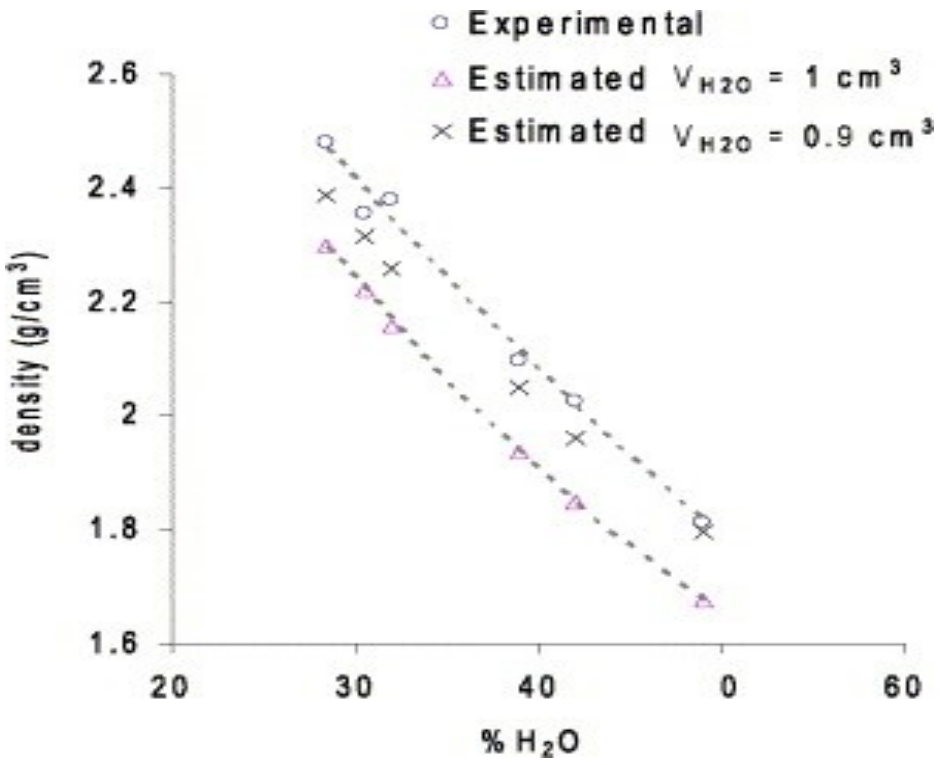

Fig. 3. Comparison between experimental and estimated densities of boehmite xerogels computed from Eq. (6) (see text). The standard deviation of experimental values is below 0.2%, which is less than the size of the symbols on the figure. The dashed lines are guides for the eye.

3.5. Pore size analysis of boehmite xerogels

Examples of nitrogen adsorption–desorption isotherms, recorded for the three kinds of xerogels are reported in Fig. 4. The nonpeptized sample (S1) gives an isotherm of type IV with an H2 hysteresis loop according to the IUPAC classification (corresponding to type E in the original de Boer classification [27]). This kind of hysteresis loop is an indication of a network of interconnected pores with narrower parts. Peptized xerogels give an isotherm of type I, with only a small hysteresis loop. This indicates that the pores are very small (micropores and small mesopores).

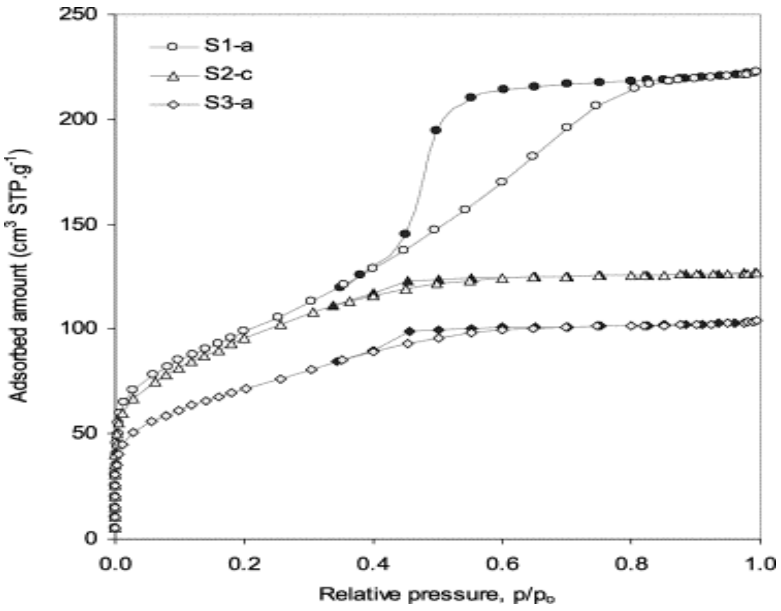

Fig. 4. Example of nitrogen adsorption isotherms, recorded at 77 K, for S1, S2, and S3 xerogels (the solid symbols denote desorption). Before analysis, the samples were outgassed under vacuum (10^{-1} Pa) at 100 °C for 20 h.

Comparative plot methods, such as the *t*-plot [28] and $*_s$-plots [29], have been revealed to be easy and powerful tools to analyze isotherms of materials containing both micro- and mesoporosity. These methods consist of plotting the amount adsorbed onto the material under study against the amount adsorbed on a reference nonporous solid. However, it has been shown that the choice of the reference isotherm is essential: it should be the isotherm of a nonporous solid, chemically similar to the substance under test [30] and [31]. In this work, we have used, as reference isotherm, the data recently published by Cejka et al. [32] for nitrogen adsorption on the nonporous Degussa Aluminumoxid C. This reference adsorbent has already been found suitable for the analysis of isotherms on porous γ-aluminas [29]. The *t*-plots corresponding to the isotherms of Fig. 4, calculated using this reference adsorbent, are shown in Fig. 5.

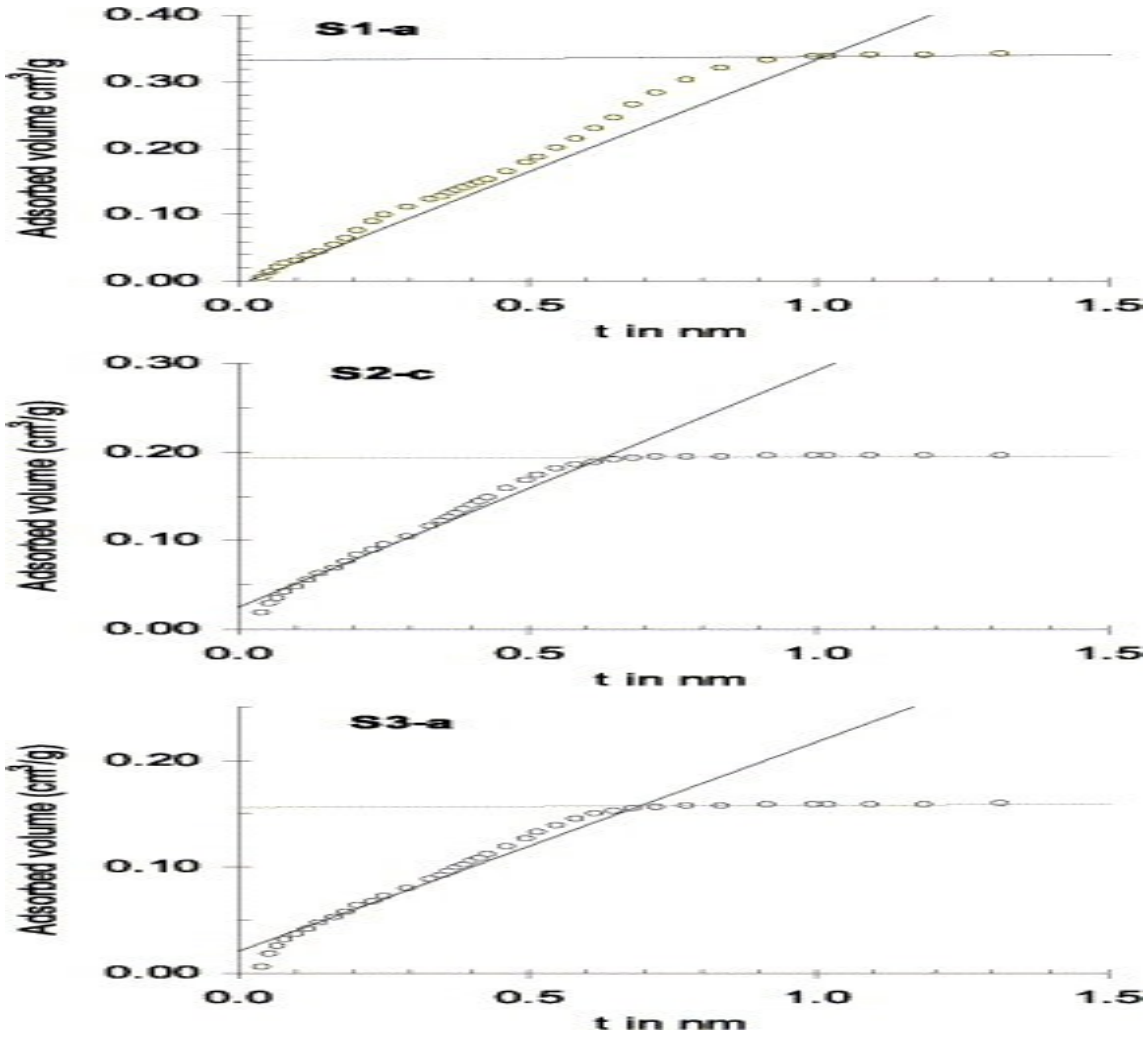

Fig. 5. *t*-plots of boehmite xerogels computed from the isotherms of Fig. 4. The nonporous Degussa Aluminumoxid C isotherm was used as reference solid (data published in Ref. [32]). The adsorbed volumes (*y* axis) are converted to the liquid equivalent volumes.

Four distinct stages can be considered in these plots. The first step, occurring in the very low pressure range (t<0.25 nm), represents the filling up of the micropores. The second step corresponds to multilayer adsorption on the meso- and macropore walls. In this stage the *t*-plot is linear because the layer-by-layer adsorption mechanism is the same as the nonporous reference one. The intercept, on the adsorption axis, of the extrapolated linear segment gives the micropore volume, denoted V_{mi}. The slope of the linear segment gives the area of the mesopore walls in addition to the external surface; this area is often denoted S_{tot} (actually S_{tot}=1000× slope, because t is in nm, the adsorbed volume in cm^3, and S_{tot} in m^2).

The third step of the *t*-plot corresponds to the occurrence of capillary condensation in the mesopores. As soon as this process starts, the *t*-plot will show an upward deviation. The last part of the *t*-plot is once more a linear segment. At this stage, all the micropores and mesopores are filled with adsorbate and the adsorption proceeds again by a multilayer mechanism as for the nonporous

reference. The intercept on the adsorption axis of the extrapolated linear segment gives the total pore volume, denoted V_{por}. The slope of the linear segment gives the area of the external surface denoted S_{ex} (S_{ex}=1000×slope). The surface and the volume of the mesopores, denoted respectively S_{meso} and V_{meso}, are given by

(7)

$$S_{meso} = S_{tot} - S_{ex} \quad \text{and} \quad V_{meso} = V_{por} - V_{mi}.$$

On the other hand, assuming a cylindrical pore geometry, an average mesopore diameter (also called hydraulic diameter), d_h, can be calculated from V_{meso} and S_{meso}:

(8)

$$\frac{V_{meso}}{S_{meso}} = \frac{\pi R^2 L}{2\pi RL} \Rightarrow d_h = 2R = 4\frac{V_{meso}}{S_{meso}}.$$

The porosity can be calculated by

(9

$$\varepsilon = \frac{\text{volume of pores}}{\text{total volume}} = \frac{V_{por}}{(V_{por} + 1/\rho)}.$$

But we cannot take for ρ the density measured for the gel before outgassing because we have seen that the density depends on the water content. However, as we know the quantity of water lost after outgassing (from the mass loss), we can calculate the estimated density using Eq. (6) (and using 0.9 cm^3 for the volume taken by 1 g of water).

All the parameters calculated from the *t*-plot are summarized in Table 2. The porosity of the peptized samples is relatively low, which indicates efficient packing of the particles, especially for S3-a. Indeed the most efficient (hexagonal) packing of uniform spheres gives an  of 0.26 with a coordination number of 12. We have seen that the boehmite nanocrystals are not spherical, but an ordered packing of monosized disks can pack at density equivalent to those of monosized spheres provided that the thickness-to-diameter ratio is close to 0.5 [33]. The porosity of S1-a corresponds to a looser packing with a coordination number of only 6. It can already be inferred that the pore distribution will be broader for S1 than for the peptized xerogels. As expected, the surface area S_{tot} decreases when the porosity decreases because a higher coordination number means more contacts between the particles.

Table 2.

Porosity parameters calculated from the *t*-plot for xerogels outgassed under vacuum (10^{-1} Pa) at 100 °C for 20 h

	H_2O (%)	S_{BET} (m^2/g)	S_{tot} (m^2/g)	V_{mi} (cm^3/g)	S_{app} (m^2/g)	V_{por} (cm^3/g)	S_{ex} (m^2/g)	S_{meso} (m^2/g)	V_{meso} (cm^3/g)	d_h (nm)	Porosity
S1	18.9	352	339	−0.000	0	0.332	5.9	333	0.332	4.0	0.44

	H_2O (%)	S_{BET} (m^2/g)	S_{tot} (m^2/g)	V_{mi} (cm^3/g)	S_{app} (m^2/g)	V_{por} (cm^3/g)	S_{ex} (m^2/g)	S_{meso} (m^2/g)	V_{meso} (cm^3/g)	d_h (nm)	Porosity
-a											
S1-b	17.8	437	370	−0.000	0	0.326	3.6	366	0.326	3.6	0.44
S2-b	22.7	363	272	0.031	86	0.202	1.2	271	0.172	2.5	0.31
S2-c	21.6	369	279	0.027	75	0.230	1.2	278	0.203	2.9	0.34
S3-a	21.8	256	197	0.020	57	0.156	2.1	195	0.136	2.8	0.26

The peptized samples contain micropores whereas, for S1 gels, the micropore volume is equal to zero (actually it is found to be slightly negative, which could reveal somewhat different surface properties between the reference solid and nanosized boehmite). The absence of micropores in nonpeptized samples confirms that these pores result from the electrostatic repulsion between the particles. The average mesopore diameter d_h is less than 3 nm for S2 and S3 gels and about 4 nm for S1.

The BET specific surface area, S_{BET}, calculated using the BET method [34] in the relative pressure range 0.06 to 0.20, is reported in Table 2. For all of the samples, this pressure range leads to the best correlation coefficient (>0.99998). There is an overestimation of S_{BET} for micropore-containing materials because the BET monolayer capacity comprises both the monolayer on the meso- and macropore surface and the amount of nitrogen that fills the micropores. The apparent surface area S_{app} corresponding actually to the micropores filling is [32]

(10)
$$S_{app}=N_A\sigma V_{mi}/V_L=2804V_{mi},$$
where N_A is the Avogadro number, σ=0.162 nm^2 is the average area occupied by one nitrogen molecule, and V_L=34.68 cm^3/mol is the molar volume of liquid N_2 at 77 K. By subtracting S_{app} from S_{BET} a better agreement is obtained with S_{tot}.

Usually the pore size distribution (PSD) of a mesoporous solid is calculated by procedures based on the Kelvin equation corrected for the statistical film thickness on the pore walls. However, it has been shown [35] that the thickness of the adsorbed film increases with the curvature of the gas-adsorbed phase interface so that the pore size, calculated from methods based on the Kelvin equation, is underestimated for small mesopores. Moreover, methods based on the Kelvin equation are not applicable to micropores because the enhancement of interaction energy in these pores is not taken into account.

Naono et al. [36], using porous silicas with known pore size, have given a correction table for cylindrical pores having a diameter in the range 2 to 4 nm. In the same way, Kruk et al. [37], using porous silica of similar structure, have shown that a simple correction of the Kelvin equation gives a pore size in a good agreement with the pore size of the model adsorbents. Very recently, Zhu et al.

[38] have proposed a method to derive the PSD from the *t*-plot. This method is applicable to both micropores and mesopores. The relationship between the statistical film thickness *t* and the pore diameter is given by an empirical equation established from samples possessing a regular cylindrical pore structure with known pore size in the range 1 to 10 nm. These various corrections for the Kelvin equation have been summarized in Fig. 6. In the relative pressure range studied by Naono (0.1 to 0.55, pore diameter from 2 to 4 nm) the agreement is rather good.

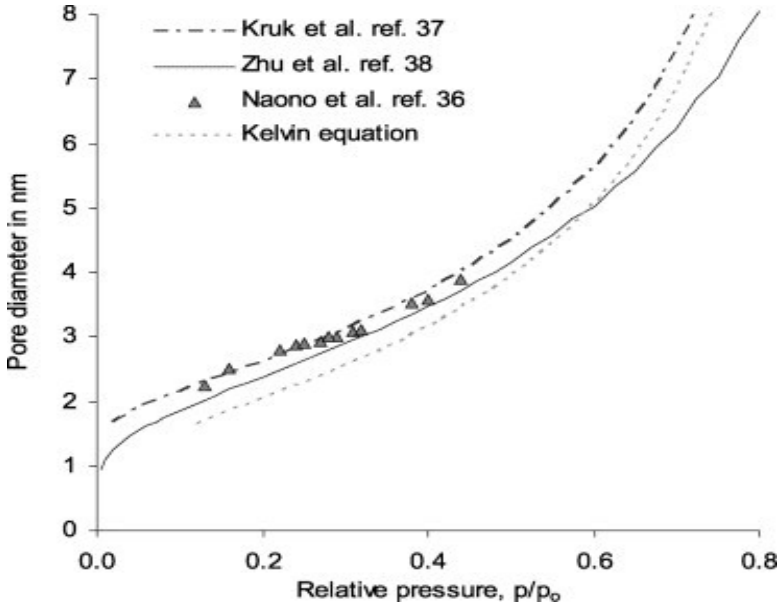

Fig. 6. Comparison between the cylindrical pore diameter calculated from the Kelvin equation (hemispherical meniscus) and some corrections proposed in the literature.

From the shape of the isotherms and the TEM images, we can reasonably assume that the pores of nanocrystalline boehmite can be considered rather cylindrical than slit-shaped. Owing to the simplicity of the correction proposed by Kruk et al., we have used the same approach to compute the PSD from our adsorption isotherms. The corrected form of the Kelvin equation for cylindrical pores, used by these authors, is

where the surface tension of nitrogen $\gamma = 8.88 \times 10^{-3}\ \mathrm{N\,m^{-1}}$and $R = 8.314\ \mathrm{J\,mol^{-1}\,K^{-1}}$. Although in cylindrical pores the hemispherical meniscus is considered to be valid only for desorption (evaporation), Kruk et al. have found that using this form of Kelvin equation for the adsorption (condensation) branch leads to the best agreement with the pore size of the model adsorbents.

The PSD shown in Fig. 7 were computed from the adsorption branch of the isotherms of Fig. 4. For the statistical film thickness $t(p/p_0)$ we have taken the values calculated from the reference isotherm already used for the *t*-plot. The curves of S2-c and S3-a have a similar shape, but the number of pores is less in S3-a, in line with a lower surface area. These distributions are monomodal but unsymmetrical with a maximum at 2.2 nm. There is almost no pore larger than 6 nm which is

expected as the isotherms present a nearly horizontal plateau above a relative pressure of 0.6. For S1-a a bimodal distribution is found, corresponding to an overlap between a peak similar to those of peptized samples and a broad unsymmetrical peak with a maximum at 4 nm. It can be noted that a rather good agreement is observed between diameter d_h (calculated from the *t*-plot) and the maximum of the PSD. Finally these distributions are consistent with an intercrystalline porosity resulting from the packing, with different densities, of monosized disks having the same dimensions than those found by XRD and TEM for boehmite nanocrystals.

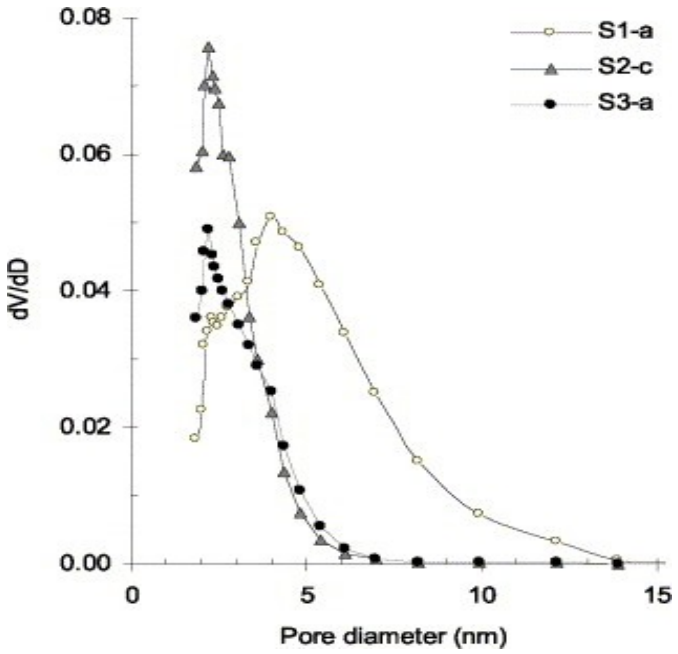

Fig. 7. Pore size distribution of boehmite xerogels calculated from the isotherms of Fig. 4 using the corrected form of the Kelvin equation for cylindrical pores proposed by Kruk et al. [37].

3.6. Effect of dehydration on the porosity of boehmite xerogels

We have seen above that peptization has a strong effect on the porosity of the boehmite xerogels prepared by hydrolysis of aluminum alkoxide. These gels were outgassed at 100 °C before the adsorption experiments but they still contained an excess of water. In this part the effect of thermal dehydration on the porosity is studied. To follow the change in porosity induced by the dehydration, boehmite xerogels were heated step by step, under vacuum (10^{-1} Pa), at increasing temperatures up to 450 °C. For each step the complete nitrogen adsorption–desorption isotherms were recorded. The loss of water was followed by weighing the sample tube after each step. The *t*-plots were calculated using Aluminumoxid C as a reference adsorbent. The porosity parameters, derived from the *t*-plot, are summarized in Table 3. This table also contains the calculated values of S_{BET}, C_{BET}, and $\%H_2O$.

Table 3.

Effect of dehydration under vacuum (10^{-1} Pa) on porosity parameters calculated from the *t*-plot

	T (°C)	S_{BET} (m^2/g)	C_{BET}	S_{tot} (m^2/g)	V_{mi} (cm^3/g)	S_{app} (m^2/g)	V_{por} (cm^3/g)	S_{ex} (m^2/g)	S_{meso} (m^2/g)	V_{meso} (cm^3/g)	d_h (nm)	H_2O (%)
S1-a	50	339	168	317	0.000	0	0.322	5.8	311	0.322	4.1	20.4
S1-a	100	352	166	339	0.000	0	0.332	5.9	333	0.332	4.0	18.9
S1-a	150	361	157	355	0.000	0	0.343	5.9	349	0.343	3.9	17.0
S1-a	200	377	149	378	0.000	0	0.359	6.2	372	0.359	3.9	14.6
S1-a	250	395	140	392	0.001	3	0.378	6.4	386	0.377	3.9	11.8
S1-a	300	417	118	396	0.005	15	0.405	7.0	389	0.400	4.1	7.5
S1-a	325	426	109	393	0.011	30	0.417	7.1	386	0.407	4.2	5.3
S1-a	355	433	103	377	0.016	46	0.426	7.4	370	0.410	4.4	3.2
S1-a	390	433	100	372	0.017	48	0.429	7.5	365	0.412	4.5	2.2
S1-a	455	430	98	366	0.018	49	0.430	7.5	359	0.413	4.6	1.6
S1-a	465	428	97	365	0.017	48	0.430	7.6	357	0.413	4.6	1.4
S2-b	30	318	114	253	0.020	56	0.175	1.1	252	0.155	2.5	25.6
S2-b	90	363	136	272	0.031	86	0.202	1.2	271	0.172	2.5	22.7
S2-b	150	381	129	287	0.031	87	0.213	1.3	286	0.182	2.6	20.7
S2-b	200	393	117	303	0.028	80	0.223	1.3	302	0.195	2.6	18.4
S2-b	250	414	105	321	0.027	77	0.236	1.4	320	0.209	2.6	15.4
S2-b	300	443	95	342	0.027	76	0.255	1.5	341	0.228	2.7	10.3
S2-b	350	477	82	362	0.027	76	0.282	1.6	360	0.255	2.8	4.2

	T (°C)	S_{BET} (m^2/g)	C_{BET}	S_{tot} (m^2/g)	V_{mi} (cm^3/g)	S_{app} (m^2/g)	V_{por} (cm^3/g)	S_{ex} (m^2/g)	S_{meso} (m^2/g)	V_{meso} (cm^3/g)	d_h (nm)	H_2O (%)
S2-b	400	481	75	371	0.024	68	0.293	1.7	369	0.269	2.9	1.9
S3-a	50	229	143	181	0.017	47	0.141	2.0	179	0.124	2.8	23.3
S3-a	100	256	151	197	0.020	57	0.156	2.1	195	0.136	2.8	21.8
S3-a	150	282	159	217	0.023	65	0.171	2.2	215	0.148	2.8	19.9
S3-a	200	297	152	225	0.025	70	0.180	2.2	223	0.155	2.8	18.3
S3-a	250	327	129	256	0.023	64	0.200	2.3	254	0.177	2.8	14.6
S3-a	305	365	106	283	0.023	64	0.225	2.5	281	0.202	2.9	8.7
S3-a	350	388	87	297	0.022	63	0.246	2.7	294	0.223	3.0	3.9
S3-a	440	382	76	292	0.020	57	0.254	2.8	289	0.234	3.2	1.4

Basically the loss of water produces an increase of all the porosity parameters. For all of the samples, below 20% H_2O, a linear relationship is observed between the pore volume and the water content (Fig. 8). The dehydration of boehmite is topotatic, which means that the transformation occurs by a short-range rearrangement with only small changes in the crystal structure. As the crystal density of AlOOH (≈3.05) is close to the crystal density of γ-Al_2O_3 (≈3.5), the increase in pore volume will essentially result from the loss of excess water. However, we found that the increase in pore volume is always significantly lower than the volume of water that is lost. For example, the pore volume of S1-a, which initially contains about 20% water, should increase up to 0.2 cm^3/g. But only half this value was measured after dehydration at 465 °C. Therefore, there is a rearrangement of the particles which get closer as the water desorbs from the surface of the crystallites. This rearrangement is easier in peptized gels in which the crystallites are more regularly stacked so that the slope of the lines in Fig. 8 is lower for S2 and S3 than for S1.

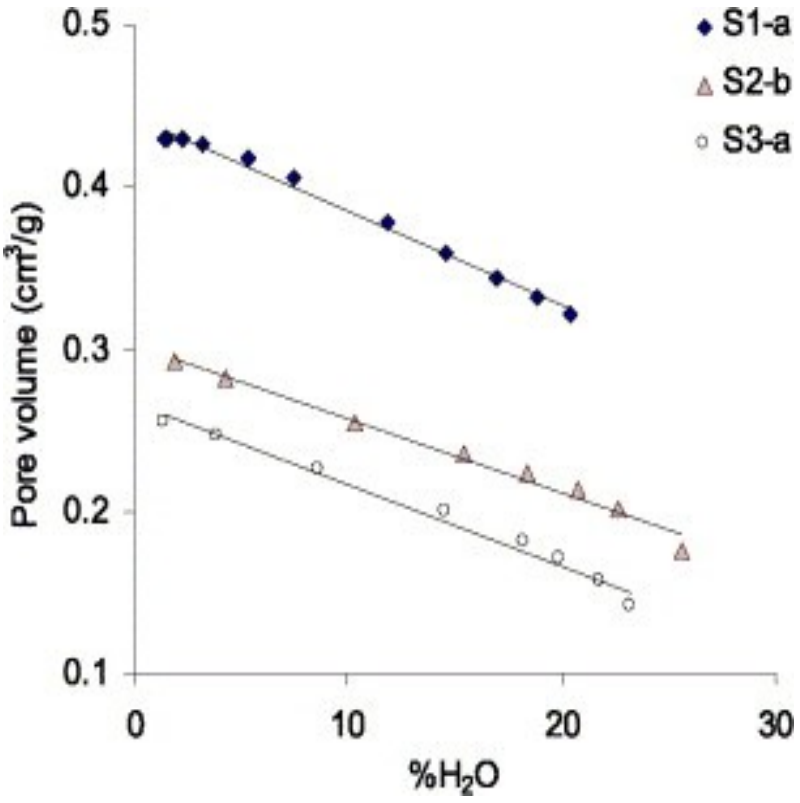
S1-a
S2-b
S3-a
Pore volume (cm³/g)
0.5
0.4
0.3
0.2
0.1
0
10
20
30
%H2O

Fig. 8. Change of mesopore volume (V_{meso}) of boehmite xerogels induced by thermal dehydration under vacuum (10^{-1} Pa).

In Fig. 9 the values of S_{BET}, S_{tot}, and V_{mi} have been plotted against the temperature. Again the trend is similar for the peptized samples but somewhat different for S1 gel for which, in the range 250 to 350 °C, a marked increase of micropore volume is observed. This temperature range corresponds to the conversion of boehmite into transition alumina. Above 350 °C the micropore volume remains constant. The theoretical intracrystalline pore volume formed during the conversion of boehmite into transition alumina can be calculated from the densities of both crystalline forms. Taking 3.05 and 3.52 g/cm^3 for boehmite and γ-Al_2O_3 respectively, gives an intracrystalline pore volume of ~0.044 cm^3/g. This value is twice as much as the micropore volume experimentally determined which suggests that many crystals shrink during the transformation which does not create internal porosity.

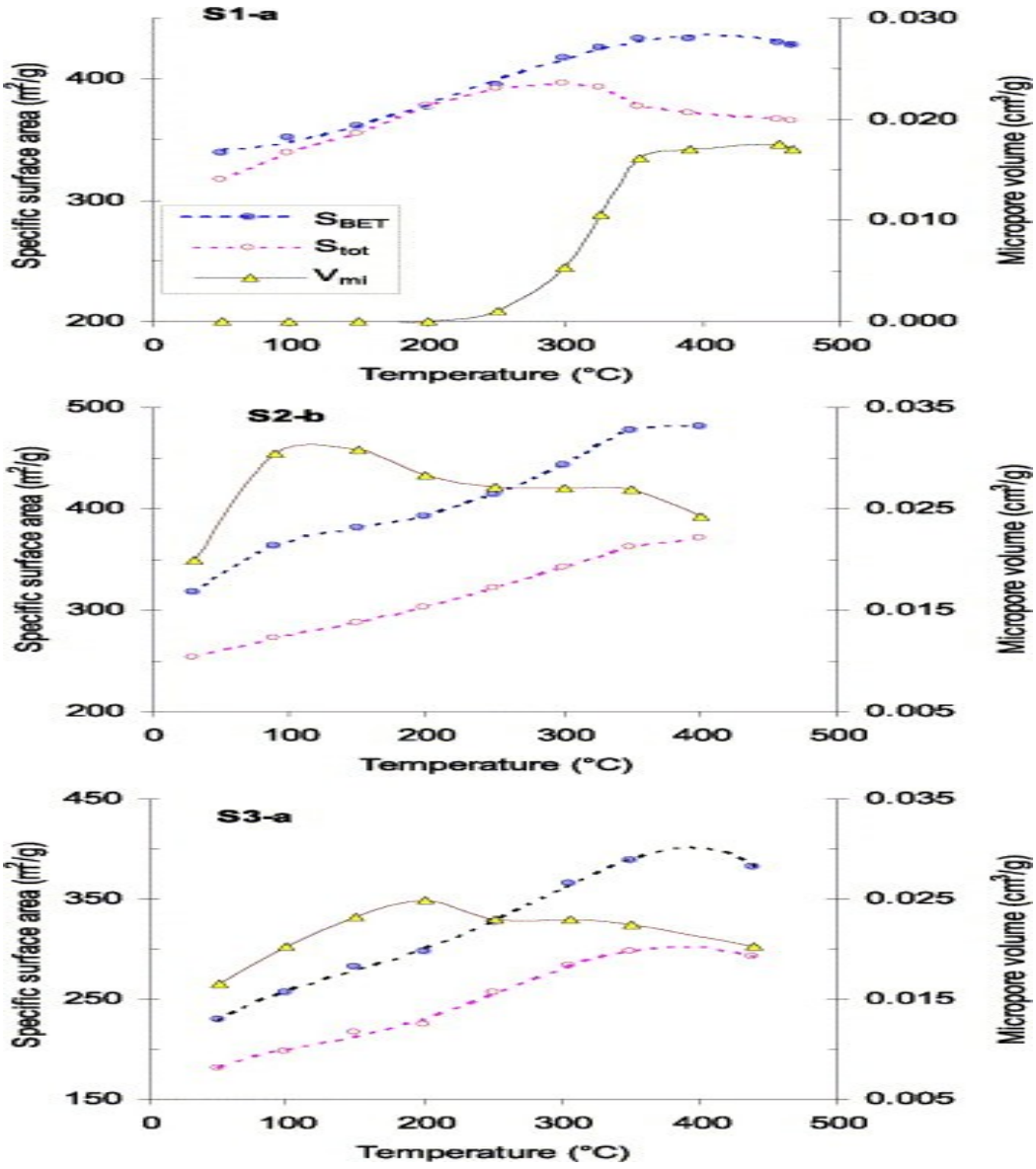

Fig. 9. Change in BET surface area (S_{BET}), total surface area (S_{tot}), and micropore volume (V_{mi}) induced by thermal dehydration of boehmite xerogels under vacuum (10^{-1} Pa).

S_{tot} is close to S_{BET} up to 300 °C, beyond which S_{tot} decreases, whereas S_{BET} still increases up to 400 °C. This discrepancy can be reduced if the presence of micropores is taken into account; actually subtracting S_{app} (calculated from Eq. (10)) from S_{BET} gives values similar to S_{tot}. The reduction of S_{tot} above 300 °C probably means that crystallite sintering begins to occur.

The peptized gels already contain micropores before dehydration. Moreover, additional micropore formation is observed when they are heated below 200 °C. Actually, below 100 °C, these micropores might already be present but still filled with water. They cannot be emptied out if the temperature is too low, even under vacuum. Beyond 150 °C the micropore volume first decreases and then remains constant between 250 and 350 °C. As stated above, these micropores result from the electrostatic repulsion created by the charges adsorbed at the surface of the particles. As these adsorbed species are expelled under the effect of temperature, the pores collapse which explains the decrease observed from 150 °C. But from 250 °C the conversion of boehmite into transition alumina begins to produce intracrystalline micropores as discussed before in the case of S1 gels. The creation of a new kind of micropores roughly balances the collapse of the first kind which explains the apparent stability observed in the range 250 to 350 °C. From 350 °C, the conversion in transition alumina is almost complete and there is no significant formation of new micropores (see graph S1-a in Fig. 9), but the collapse of the intercrystalline micropores still occurs, which explains the decrease observed beyond 350 °C for peptized samples. For these gels, S_{BET} increases steadily with temperature up to 400 °C. S_{tot} follows a similar trend but always remains lower than S_{BET}. At low temperatures, the gap between them can be accounted for micropore filling, but from 300 °C, this is no longer possible. This difference increases with the surface area but, in any case, it is always less than 10%.

The decrease of S_{tot}, most likely resulting from the sintering of particles, occurs from 300 °C for S1 gels but only from 400 °C for peptized samples. This difference is probably due to the intercrystalline micropores which prevent the contact between particles and consequently delay the sintering.

For all samples, we found that C_{BET} depends on the water content. Plotting C_{BET} against $\%H_2O$ (Fig. 10) shows that for high water content, C_{BET} first increases with the loss of water, and then C_{BET} decreases almost linearly. This decrease shows that the adsorption energy of N_2 is higher on a water-covered surface of boehmite. The C_{BET} increase for high water content is observed for gels containing more than 20% of water. In these samples part of the water is probably adsorbed in a multilayer, which can lower the adsorption energy of nitrogen.

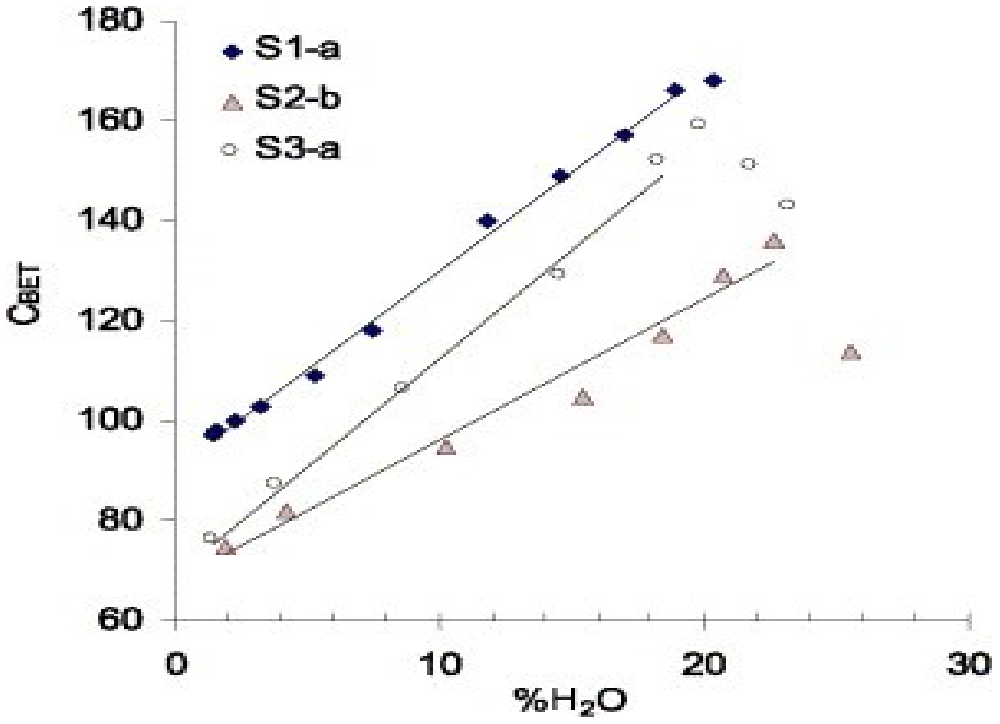

Fig. 10. Correlation between BET constant (C_{BET}) and water content of xerogels.

The effect of the heating on the PSD (calculated using the same correction as Kruk et al. [37]) is shown in Fig. 11. For all samples, as a general trend, dehydration increases the number of pores. For S1 gels the peak at 2.2 nm increases more than the broad peak at 4 nm. Above 200 °C a shift of this peak toward larger pore size is observed.

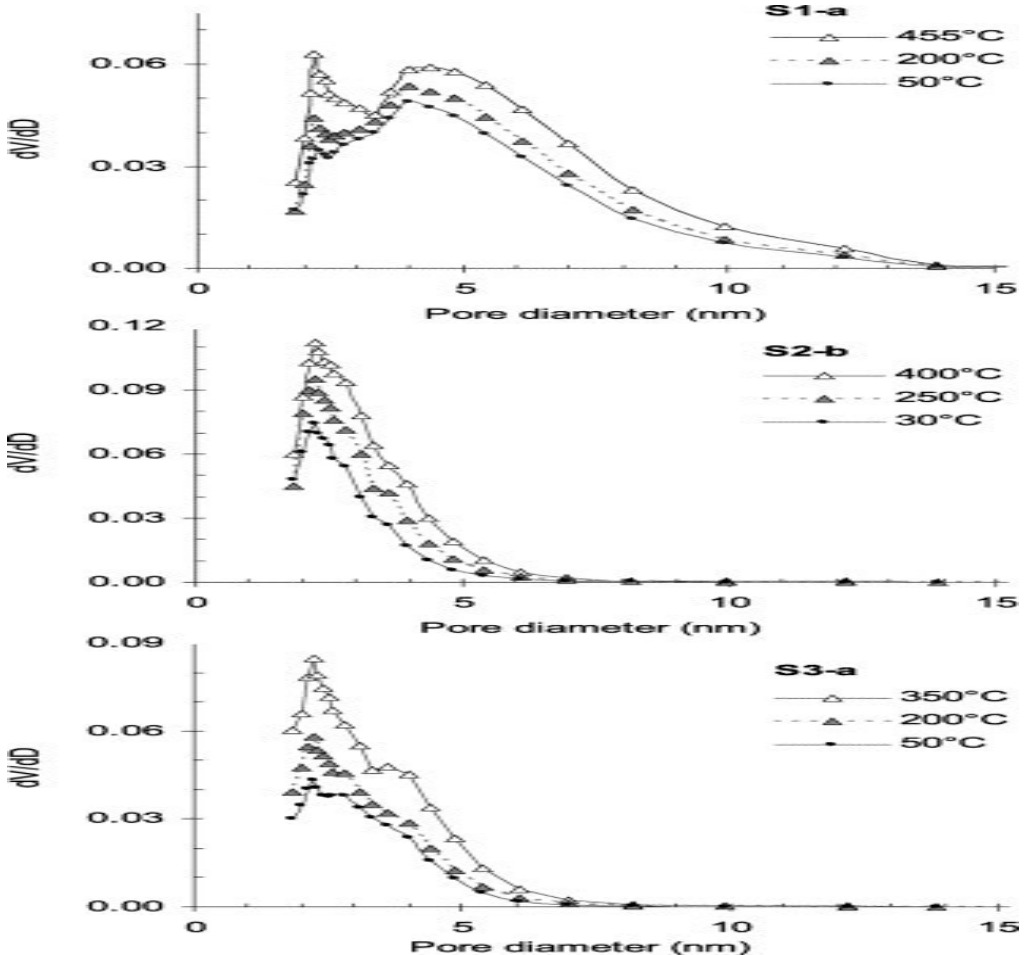

Fig. 11. Effect of thermal dehydration under vacuum (10^{-1} Pa) on pore size distribution of xerogels calculated using the corrected form of the Kelvin equation for cylindrical pores proposed by Kruk et al. [37].

For S2 gel, a slight shift of PSD toward larger pore size with no significant change in shape is observed. For S3 gel the PSD becomes bimodal with the growth of a new peak at 3.6 nm.

The dehydration temperature under vacuum could not exceed 465 °C because our sample tubes are made of Pyrex glass. At this temperature, transition alumina still contains more than 1% water. To reach a lower amount, some samples have been heated under air up to 800 °C.

From 450 °C the lines of boehmite are no longer visible on the XRD patterns. Whole pattern fitting with a model based on a cubic spinel-type structure (space group No. 227, $Fd\bar{3}m$) gives good agreement with experimental patterns. There is almost no tetragonal deformation, which suggests that these patterns could correspond to η-alumina [39]. No sign of the formation of δ- or θ-alumina was detected up to 800 °C and the cell parameter did not change over the whole temperature range (a=0.792±0.001 nm). Though crystal structure remains unchanged, the lines become narrow as the temperature increases, which indicates crystal growth. For example, in the case of S3-a gel, the ordering domain estimated from the FWHM of the (400) reflection increases from 2.5 nm (450 °C) to 4.1 nm (800 °C).

The *t*-plots were calculated from the adsorption isotherms of the xerogels heated in air. The porosity parameters, derived from the *t*-plot, are summarized in Table 4. The first rows of Table 4 show the effect of heating at atmospheric pressure instead of under vacuum. S_{BET} and S_{tot} are reduced by 14% and V_{mi} decreases by 21%. This effect can be explained by the fact that the steam produced during the dehydration is quickly evacuated under vacuum whereas it remains trapped in the mesopores at atmospheric pressure. This water vapor inhibits the boehmite dehydration [40] and [41] but also induces crystal growth by hydrothermal reaction.

Table 4.

Effect of dehydration on porosity parameters calculated from the *t*-plot for the S2-a xerogel

Outgassing conditions	***T*** **(°C)**	S_{BET} **(m^2/g)**	C_{BET}	S_{tot} **(m^2/g)**	V_{mi} **(cm^3/g)**	S_{app} **(m^2/g)**	V_{por} **(cm^3/g)**	S_{ex} **(m^2/g)**	S_{meso} **(m^2/g)**	V_{meso} **(cm^3/g)**	d_h **(nm)**
Vacuum	450	468	72	393	0.013	38	0.324	3.3	390	0.311	3.2
Air–2 h	500	333	61	284	0.006	17	0.291	3.0	281	0.285	4.1
Air–2 h	700	237	72	209	0.004	10	0.275	3.2	206	0.271	5.3
Air–2 h	800	171	97	152	0.005	14	0.261	3.3	149	0.256	6.9
Air–10 h	800	154	101	131	0.006	18	0.263	3.4	128	0.257	8.0
Air–2 h	1400	2.8	104								

The PSD reported in Fig. 12 demonstrates that the thermal treatment under air, in the range from 500 to 800 °C, has a strong effect on the porosity. As the temperature increases there is a broadening of the distribution and a marked decrease of small pores (below 3 nm). However, even after a treatment at 800 °C, micropores are still present and their volume does not seem to shrink even after a calcination for 10 h (Table 4).

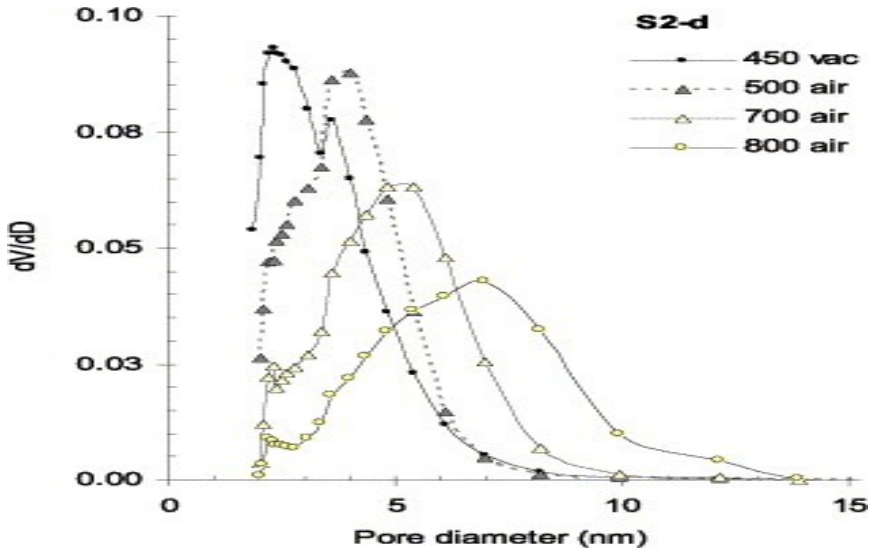

Fig. 12. Effect of thermal dehydration in air on pore size distribution of an S2-type xerogel calculated using the corrected form of the Kelvin equation for cylindrical pores proposed by Kruk et al. [37].

As previously, C_{BET} was found to depend on the water content, but in the opposite way; C_{BET} is minimal for the samples heated at 500 °C and for higher temperatures it increases again.

4. Summary

Boehmite xerogels were prepared according to the Yoldas process, using various amounts of acid for the peptization ($H^+/Al = 0$, 0.07, 0.2). XRD patterns and TEM micrographies show that these gels are made of nanosized crystals in the shape of platelets or disks, 5–9 nm in width and 3 nm thick. According to the amount of acid, no significant differences are found in size and shape but in the spatial arrangement of the crystallites. Nonpeptized gels give nitrogen adsorption–desorption isotherms of type IV with an H2 hysteresis loop according to the IUPAC classification whereas peptized gels give isotherms nearly of type I with only a small hysteresis loop. The adsorption isotherms are analyzed by the *t*-plot method, using Degussa Aluminumoxid C as reference adsorbent. It is found that the majority of pore volume results from intercrystalline mesopores, but the peptized gels also contain micropores, probably due to the space created by the electrostatic repulsion between the protons bonded to the surface hydroxyl groups. The values of the porosity reveal that the particle packing is nearly hexagonal for the gel peptized with the larger amount of acid (porosity = 0.26), whereas it is less dense in nonpeptized gel (porosity = 0.44).

When boehmite xerogels are heated under vacuum, from 250 °C onward an intracrystalline microporosity is created, resulting from the dehydration into transition alumina. On the other hand, heating causes the desorption of chemisorbed water and the collapse of intercrystalline micropores.

The microporosity leads to overestimation of the BET specific surface area and the total surface S_{tot}, calculated from the *t*-plot, gives a more reliable value. This surface area increases up to a limit temperature (300 °C for nonpeptized gels and 400 °C for peptized gels) beyond which sintering of the particles begins and the surface decreases.

The PSD were calculated assuming a cylindrical pore geometry and using the corrected Kelvin equation proposed by Kruk et al. [37]. Peptized xerogels have a monomodal unsymmetrical distribution with a maximum near 2 nm and no pores larger than 6 nm. Nonpeptized gels have a bimodal distribution corresponding to an overlap between a narrow peak near to 2 nm and a broad unsymmetrical peak with a maximum at 4 nm. Heating under vacuum up to 400 °C increases the number of pores and the pore distributions are shifted toward larger pore size except for the gel peptized with $H^+/Al = 0.07$, which shows very good thermal stability.

Heating in air above 400 °C has a strong effect on the porosity. As the temperature increases there is a broadening of the distribution and a marked decrease of small pores (below 3 nm). However, even after a treatment at 800 °C, micropores are still present.

The BET constant, C_{BET}, decreases almost linearly during the dehydration down to about 1% of residual water then C_{BET} increases again on further dehydration. Thus the adsorption energy of nitrogen is lower on transition alumina compared to boehmite or corundum.

Acknowledgement

This research was done in the frame of the MINIREF (ENK6-CT-2001-00515) project supported by the E.C.

References

K. Wefers, G.M. Bell, Oxides and Hydroxides of Aluminium, Alcoa Technical Paper, No. 19, Alcoa Laboratories, 1987.

R.B. Bagwell and G.L. Messing In: D.-M. Liu, Editor, *Porous Ceramic Materials*, *Key Eng. Mater.* 115 (1996), pp. 45–64.

R.T. Tettenhorst and D.A. Hofmann, *Clays Clay Miner.* 28 (1980), pp. 373–380.

R.T. Tettenhorst and C.E. Corbato, *Clays Clay Miner.* 36 (1988), pp. 181–183.

M. Bellotto, B. Rebours and P. Euzen, *Mater. Sci. Forum* 278–281 (1998), pp. 572–577.

X. Bokhimi, J.A. Toledo-Antonio, M.L. Guzman-Castillo and F. Hernandez-Beltran, *J. Solid State Chem.* 159 (2001), pp. 32–40.

A.E. Gobichon, B. Rebours and P. Euzen, *Mater. Sci. Forum* 378–381 (2001), pp. 523–528.

B.C. Lippens, Structure and Texture of Aluminas, Thesis, Delft, 1961.

S.J. Wilson, *J. Solid State Chem.* 30 (1979), pp. 247–255.

T. Tsuchida, R. Furuich and T. Ishii, *Thermochim. Acta* 39 (1980), pp. 103–115.

J. Rouquerol, F. Rouquerol and M. Ganteaume, *J. Catal.* 36 (1975), pp. 99–110.

B.E. Yoldas, *J. Mater. Sci.* 10 (1975), pp. 1856–1860.

B.E. Yoldas, *Am. Ceram. Soc. Bull.* 54 (1975), pp. 286–288.

B.E. Yoldas, *Am. Ceram. Soc. Bull.* 54 (1975), pp. 289–290.

B.E. Yoldas, U.S. Patent 3,941,719, 1976.

B.R. Baker and R.M. Pearson, *J. Catal.* 33 (1974), pp. 265–278.

T. Tsukada, H. Segawa, A. Yasumori and K. Okada, *J. Mater. Chem.* 9 (1999), pp. 549–553.

X. Bokhimi, J.A. Toledo-Antonio, M.L. Guzman-Castillo, B. Mar-Mar, F. Hernandez-Beltran and J. Navarrete, *J. Solid State Chem.* 161 (2001), pp. 319–326.

K. Okada, T. Nagashima, Y. Kameshima, A. Yasumori and T. Tsukada, *J. Colloid Interface Sci.* 253 (2002), pp. 308–314.

G.G. Christoph, C.E. Corbato, D.A. Hofmann and R.T. Tettenhorst, *Clays Clay Miner.* 27 (1979), pp. 81–86.

W.O. Milligan and H.B. Weiser, *J. Phys. Colloid Chem.* 55 (1951), pp. 490–496.

J. Campaniello, P. Berthet, F. D'Yvoire and A. Revcolevschi, *J. Mater. Res.* 10 (1995), pp. 297–301.

A.F. Popa, S. Rossignol and C. Kappenstein, *J. Non-Cryst. Solids* 306 (2002), pp. 169–174.

D. Fauchadour, F. Kolenda, L. Rouleau, L. Barre and L. Normand, *Stud. Surf. Sci. Catal.* 143 (2002), pp. 453–461.

C.R. Evanko, R.F. Delisio, D.A. Dzombak and J.W. Novak Jr., *Colloids Surf. A Physicochem. Eng. Aspects* 125 (1997), pp. 95–107.

B.A. Hendriksen, D.R. Pearce and R. Rudham, *J. Catal.* 24 (1972), pp. 82–87.

J.H. de Boer In: D.H. Everett and F.S. Stone, Editors, *The Structure and Properties of Porous Materials, Proceedings of the 10th Symposium of the Colston Research Society*, Butterworths, London (1958), pp. 68–94.

B.C. Lippens and J.H. De Boer, *J. Catal.* 4 (1965), pp. 319–323.

K.S.W. Sing In: D.H. Everett and R.H. Ottewill, Editors, *Surface Area Determination, Proc. Int. Symp. 1969*, Butterworths, London (1970), p. 25.

S.J. Gregg and K.S.W. Sing, Adsorption, Surface Area and Porosity, Academic Press, London (1982).

M. Jaroniec and K. Kaneko, *Langmuir* 13 (1997), pp. 6589–6596.

J. Cejka, N. Zilkova, J. Rathousky, A. Zukal and J. Jagiello, *Langmuir* 20 (2004), pp. 7532–7539.

R.M. German, *Particle Packing Characteristics, Metal Powder Industries Federation*, Princeton, NJ (1989).

S. Brunauer, P.H. Hemmett and E. Teller, *J. Am. Chem. Soc.* 60 (1938), pp. 309–319.

H.Y. Zhu, G.Q. Lu and X.S. Zhao, *J. Phys. Chem. B* 102 (1998), pp. 7371–7376.

H. Naono, M. Hakuman and T. Shiono, *J. Colloid Interface Sci.* 186 (1997), pp. 360–368.

M. Kruk, M. Jaroniec and A. Sayari, *Langmuir* 13 (1997), pp. 6267–6273.

H.Y. Zhu, P. Cool, E. Vansant, B.L. Su and X. Gao, *Langmuir* 20 (2004), pp. 10,115–10,122.

P. Alphonse and M. Courty, *Thermochim. Acta* 425 (2005), pp. 75–89.

C. Eyraud and R. Goton, *J. Chim. Phys.* 51 (1954), pp. 430–433.

W.D. Callister Jr., I.B. Cutler and R.S. Gordon, *J. Am. Ceram. Soc.* 49 (1966), pp. 419–422.

Corresponding author.